3Mor2A-07, IEEE Trans. Appl. Supercond.

Nb_3Sn wire fabrication using rod-in-tube method with a diffusion couple of Nb and Sn alloy with co-addition of Cu and Zn

Nobuya Banno, Koki Asai, and Tsuyoshi Yagai

***Abstract*—Large-scale devices, such as the next generation high energy particle accelerator project, demand the enhancement of the J_c and cost performance of Nb_3Sn wires. The cost performance is closely related to the design and drawability of the wires. This study aims to increase the hardness of the soft Sn core of the wires through the precipitation of fine compound particles, improve the hardness balance between the constituent materials (Nb, Cu, and Sn), and investigate the feasibility of this method for practical wire drawing. First, we investigated the variations in microstructure and hardness when Cu and Zn were co-added to Sn. A total addition of 50% Cu–Zn to the Sn alloy can triple the hardness, leaving the alloy ductile enough to sustain the entire deformation process. Subsequently, we manufactured tube-type multifilamentary wires using subelements containing different types of Sn alloys, with and without an intermediate layer of Cu between Sn and Nb. In the absence of Cu, we observed the formation of a large area of Nb_6Sn_5, which is responsible for the formation of a large coarse Nb_3Sn grain area. The presence of Cu suppresses the formation of the Nb_6Sn_5, demonstrating that controlling the Cu/Sn ratio at the subelement level is critical to suppressing the formation of coarse Nb_3Sn areas.**

***Index Terms*— Hardness, Microstructure, Nb_3Sn, Sn alloy, Zn.**

I. INTRODUCTION

LARGE-SCALE devices, such as next-generation high-energy particle accelerators and fusion reactors, require extremely large numbers of superconducting wires [1][2],[3],[4],[5],[6]. Therefore, the realization of these projects necessitates the enhancement of wire performance as well as cost effectiveness. Currently, high-performance Nb_3Sn wires are of the internal tin type[7],[8],[9],[10],[11], tube-type[12],[13], [14] and powder-in-tube type with internal oxidation processes[15],[16],[17],[18]. The performance of the internal tin and tube-type Nb_3Sn wires is approaching the required J_c for the Future Circular Collider (FCC) project (1500 A/mm^2 at 16T)[1],[2],[3]. Furthermore, the internal oxidation of Nb_3Sn wires exceeds the stipulated requirement for this project[19]. Meanwhile, the FCC magnets are designed to incorporate several thousand tons of Nb_3Sn wiring, amounting to thousands of millions of euros. Therefore, enhancing the cost performance of the Nb_3Sn wires by a small percentage would lead to cost savings of tens of millions of euros.

Cost performance is closely related to the wire design and drawability. Good drawability can mitigate the risk of wire breakage and improve the yield rate. Furthermore, a good hardness balance would contribute to the maintenance of a good cross-sectional shape. The Nb_3Sn precursor composite comprised Cu, Nb, and soft Sn. The hardness of Sn is less than one-sixth of that of Cu or Nb. As the composite is deformed, the difference in hardness increases. Empirically, this hardness imbalance is often considered to be the primary cause of irregular deformation during the drawing process.

In this study, various Sn alloys were fabricated by the co-addition of Cu and Zn. Their microstructures, compositions, and hardnesses were investigated. Zn may have dispersed the compound precipitate. Tube-type multifilamentary wires are manufactured using Sn alloys. The feasibility of using hardened Sn alloys was investigated through microstructural observations of phase formation behavior and critical current measurements.

II. EXPERIMENTAL

A. Casting of Sn Alloy

The Sn alloys were cast in a normal induction-heating furnace in an Ar atmosphere. Cu, Zn, and Ti were used as additive elements. A mixture was prepared by combining predetermined amounts of each constituent material. For the addition of Ti, titanium powders (– 325 mesh) were utilized. The mixture was heated to a temperature range of 500 to 900 °C, which is above the melting point of Sn-alloys, and maintained for a sufficient duration to ensure the complete dissolution of Ti.

B. Microstructural and Microchemical Analysis

The microstructures of the samples were observed using a field-emission scanning electron microscope (FESEM), and composition analysis was performed using energy-dispersive X-ray spectroscopy (EDS) with the FESEM. The cross-section was first polished with polycrystalline diamond suspensions

Manuscript received 25 September 2024.

This work was supported in part by JSPS KAKENHI Grant Number JP23K04453. *(Corresponding author: Nobuya Banno.)*

N. Banno is with the Research Center for Energy and Environmental Materials, National Institute for Materials Science, Tsukuba, Ibaraki 305-0047, Japan (e-mail: banno.nobuya@nims.go.jp).

Koki Asai is with Sophia University, Tokyo 102-8854, Japan, and with the National Institute for Materials Science, Tsukuba, Ibaraki 305-0047, Japan (e-mail: kouki0204@eagle.sophia.ac.jp).

T. Yagai is with Sophia University, Tokyo 102-8554, Japan. (e-mail: tsuyoshi-yagai@sophia.ac.jp).

and then polished with non-crystallizing amorphous 0.05 and 0.02 μm colloidal silica suspensions (MasterMet, Buehler) in the final steps.

The hardness of the Sn alloys was measured using a Micro-Vickers hardness tester at a force of 0.025 kgf.

C. Wire Fabrication

Two configurations of the tube-type subelement were fabricated, distinguished by the presence of an additional copper layer between the Nb-alloy tube and the central Sn-alloy bar. In Configuration 1, the Sn-alloy bar, swaged to a diameter of 2.7 mm, was inserted into the Nb tube with an outer/inner diameter of 5.8/3.0 mm. This composite was then inserted into a Cu tube with an outer/inner diameter of 8.0/6.0 mm. This single-core composite was swaged and drawn into a hexagonal wire 1.0 mm in height. Nineteen pieces of the hexagonal single-core wires were stacked into a Cu tube with an outer/inner diameter of 8.0/5.3 mm and subsequently drawn into a wire 1.09 mm in diameter.

In Configuration 2, a thin Cu layer was incorporated between the Nb and the Sn alloy. The Sn alloys, swaged into a bar with a diameter of 8.5 mm, was inserted into a Cu tube with an outer/inner diameter of 10.0/9.0 mm. The Sn/Cu rod was then deformed to a final diameter of 2.7 mm. The subsequent steps for producing the subelement and the multifilamentary wire were the same as those followed for the Configuration 1. The final wire was a multifilamentary wire with 19 filaments and 1.09 mm in diameter.

Each sample was encased in a quartz tube filled with argon gas. The encased samples were heat treated at 650 ºC/100 h with a ramp-up time of 4 h for Nb_3Sn phase formation. To observe the temporal evolution of the microstructure, the samples were removed from the furnace at 400, 500, 600, and 650 ºC, as well as at 650 ºC/20 h and 650 ºC/50 h. At the extraction from the oven, the sample had been immediately quenched in water.

C. I_c Measurement

I_c was measured for short samples (4 cm in length) using the standard four-point probe method. The voltage tap distance was 10 cm and the I_c was determined by an electric criterion of 1 μV/cm. The non-Cu J_c was calculated by dividing the I_c by the non-Cu area.

III. Results and Discussion

A. Microstructure and Hardness of Sn Alloys

The compositions of the cast Sn alloys are summarized in Table I, and the backscattered electron (BSE) images of the microstructures of typical Sn alloys are shown in Fig. 1. In Sn–2Ti, typically, Ti_6Sn_5 with a size of approximately 4 μm precipitates [20]. For a 20% Cu composition, the microstructure shows an island-like microstructure with tiny η-CuSn particles dispersed. However, Sn–50Cu exhibited a dendritic microstructure with ε-CuSn phase growth and became markedly brittle due to its excessive Cu content. In Sn–20Cu–30Zn–2Ti and Sn–10Cu–40Zn–2Ti, there was no dendritic structure; however, a microstructure with dispersed compound particles was observed. EDS analysis indicated that these compounds are β-CuZn and γ-CuZn in Sn–20Cu–30Zn–2Ti and Sn–10Cu–40Zn–2Ti, respectively. According to the phase diagram of Cu–Zn, the composition ratios of Cu and Zn in these alloys are close to those of β-CuZn and γ-CuZn, respectively. The melting points of these phases were approximately 900 and 830 °C, respectively. Therefore, β-CuZn and γ-CuZn are stable in the Sn alloy; hence, they would precipitate as embryos during cooling. Notably, Zn does not dissolve in Sn. Thus, β-CuZn and γ-CuZn are presumed to have precipitated preferentially. The particle size ranged from approximately 10 to 20 μm.

In Sn–20Cu, the embryo is η-CuSn as mentioned above. The particle size was less than 8 μm. If 5 at% of Zn is added, the particle size is further reduced to almost less than 5 μm, and the particles are more dispersed. EDS revealed that the precipitates originated from ε-CuSn containing Zn. The Cu:Zn:Sn composition ratio is approximately 58:14:28. Zn appears to be effective in suppressing the growth of ε-CuSn. In Sn–10Cu–5Zn, the embryo was believed to be β-CuSn; Cu:Zn:Sn is approximately 53:38:9.

Fig. 2 summarizes the Vickers hardness values of the as-cast Sn alloys with those of Nb and Cu as references. The hardness of practically-used Sn–2Ti is approximately 11 HV, which is almost one-sixth that of Nb and Cu. The addition of large

TABLE I
Composition (at%) of Casted Sn Alloys

Name	Sn	Cu	Zn	Ti	Ductility
Sn–2Ti	98	0	0	2	Good
Sn–20Cu	80	20	0	0	Good
Sn–50Cu	50	50	0	0	Brittle
Sn–20Cu–30Zn–2Ti	48	20	30	2	Good
Sn–10Cu–40Zn–2Ti	48	10	40	2	Good
Sn–31Zn	69	0	31	0	Good
Sn–10Cu–5Zn	90	10	5	0	Good
Sn–20Cu–5Zn	75	20	5	0	Good

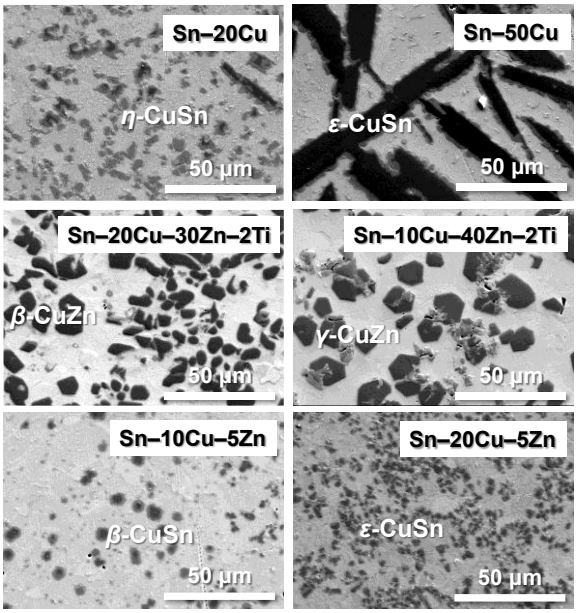

Fig. 1. BSE images of typical Sn alloys.

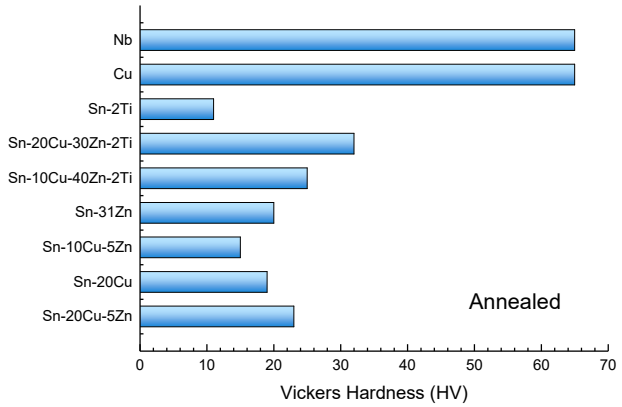

Fig. 2. Comparison of the Vickers hardness of Nb, Cu, and Sn alloys.

amounts of Cu and Zn can triple this hardness. After the drawing process (true strain = 8.14), the Vickers hardnesses of Nb, Cu and Sn-alloy were nearly saturated at 167, 133 and 32 Hv for Sn–20Cu–30Zn–2Ti wire, and 165, 136 and 33 Hv for Sn–10Cu–40Zn–2Ti wire, respectively.

B. Phase Formation Behavior

Cross-sectional views of the multifilamentary wires fabricated using Sn–20Cu–30Zn–2Ti are shown in Fig. 3. Drawability was good until the Sn core size was reduced to approximately 50 μm, at which point wire breakage often occurred. The size limitation may depend on the size of the precipitate.

Fig. 4 shows the phase formation at the interface between Nb and Sn–20Cu–30Zn–2Ti of the sub-element in the multifilamentary wires in Fig. 3(a). The precipitated β-CuZn remained in the Sn alloy core at the temperature of 650 °C and $NbSn_2$ was formed at the interface (Fig. 4(a)). After 20 h at 650 °C, the Nb_2Sn decomposed into Nb_6Sn_5 and Sn and a thin reaction layer of fine-grained (FG) Nb_3Sn layer formed at the reaction front (Fig. 4(b)). After 20 h at 650 °C, the Nb_6Sn_5 decomposed into coarse-grained (CG) Nb_3Sn and Sn(Cu, Zn),

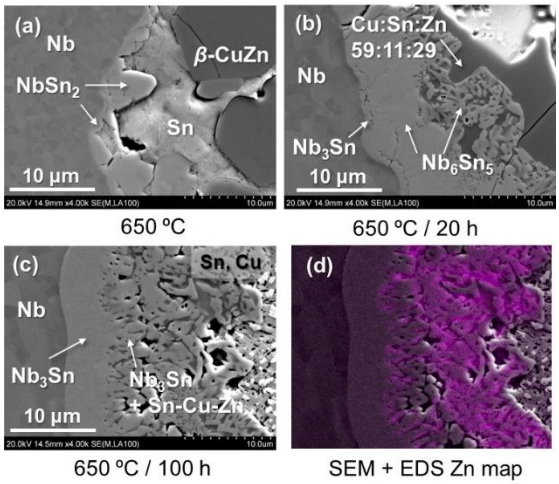

Fig. 4. Phase formation between Nb and Sn-20Cu-30Zn-2Ti of the subelement in the multifilamentary wire (configuration 1) at (a) 650 °C, (b) 650 °C/20 h and (c) 650 °C/100 h, and (d) EDS Zn map.

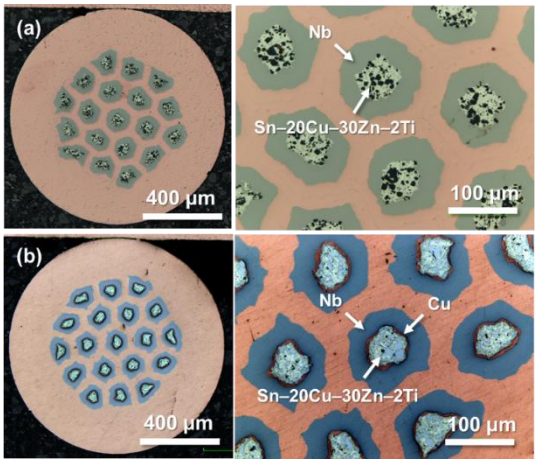

Fig. 3. Cross-sectional views of the multifilamentary wires using Sn–20Cu–30Zn–2Ti: (a) Configuration 1 (without Cu layer between Nb and Sn alloy) and (b) Configuration 2 (with Cu layer).

while the FG Nb_3Sn layer grew further (Fig. 4(c)). Zn does not dissolve in Nb_3Sn as reported in[21] (Fig. 4(d)). This phase formation behavior is similar to the case in which Sn activity is significantly high[22],[23],[24],[25]. In general, in Sn–Cu, the Sn activity increases with the Sn content in Sn–Cu. At Sn content ratios (Sn/(Sn + Cu)) greater than 25at%, reportedly, $NbSn_2$ and Nb_6Sn_5 forms before Nb_3Sn[23].

To reduce the Sn content, a thin Cu layer was inserted between Nb and the Sn alloy in the second configuration (Fig. 3(b)). Fig. 5 shows the phase formation in this wire when a thin intermediate Cu layer exists between Nb and Sn–20Cu–30Zn–2Ti. The Sn/(Sn + Cu + Zn) ratio decreased from 50at% to 33at%. The layer growth of Nb_6Sn_5 (decomposed from $NbSn_2$) was suppressed compared to the case without Cu (Fig. 5(a) and (b)). As reported by Xu, an increase in the Cu content resulted in an increase in the FG/CG ratio [22]. This accounts for the small Nb_6Sn_5 layer growth in configuration 2 (Fig. 5(c)). Nb_6Sn_5 did not transform into coarse Nb_3Sn; instead, a Nb–Sn–Ti–Cu–Zn compound phase was formed (Fig. 5(d)). EDS

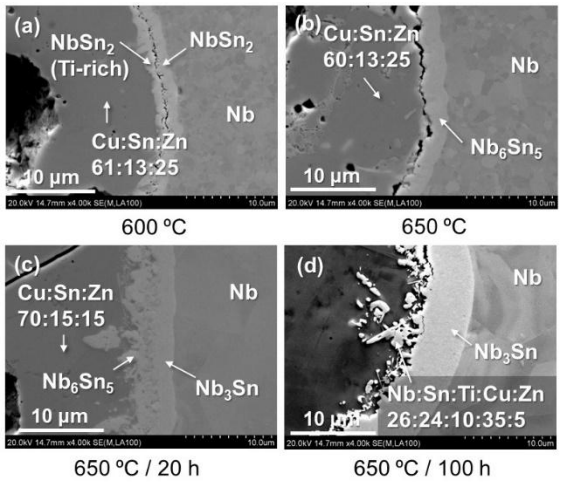

Fig. 5. Phase formation between Nb and Sn–20Cu–30Zn–2Ti in the presence of a thin intermediate Cu layer in the multifilamentary wire (configuration 2) at (a) 600 °C, (b) 650 °C, (c) 650 °C/20 h, and (d) 650 °C/100 h.

indicated a Nb:Sn:Ti:Cu:Zn composition ratio of 26:24:10:35:5. The formation of complex compound phases is often observed when Ti is doped to Sn[26].

Fig. 6 shows the grain morphologies of the FG area in configurations 1 and 2. The average grain size was calculated by dividing by the number of grains in a certain area containing more than 140 grains, which is a reasonable number from a statistical standpoint. The average grain sizes were 144 and 114 nm, respectively. Notably, the insertion of a Cu layer resulted in a finer grain morphology. In addition, at a high Sn content (configuration 1), finer grains were observed near the Nb side, whereas at a high Cu content (configuration 2), the grains tended to be finer near the Sn alloy core side.

C. Effect of Zn Addition

Fig. 7 compares the grain morphologies of the FG Nb_3Sn area with those of Sn–20Cu–30Zn–2Ti and Sn–10Cu–40Zn–2Ti in configuration 2. A reduction in the Cu–Zn ratio, as in Sn–10Cu–40Zn–2Ti, resulted in a thicker Nb_3Sn layer. Zn has been reported to be an effective element for promoting Nb_3Sn formation[27]. The increased Zn content is believed to enhance the formation of Nb_3Sn.

D. Non-Cu J_c Properties

Fig. 8 shows the non-Cu J_c properties of the multifilamentary wires fabricated using Sn–20Cu–30Zn–2Ti and Sn–10Cu–40Zn–2Ti. The non-Cu J_c properties were measured for configurations 1 and 2. The J_c values are considerably lower than those of industrial wires[22],[24],[28],[10], which may be because the heat treatment conditions were not optimized and Sn diffusion was not sufficient owing to the large sub-element diameter. Otherwise, Ti might not diffuse sufficiently in Nb_3Sn because of the presence of Nb–Sn–Ti–Cu–Zn or Nb_6Sn_5, as shown in Fig. 4 and 5. As shown in Fig. 8, the J_c of the Sn–10Cu–40Zn–2Ti sample was higher than that of the Sn–20Cu–30Zn–2Ti sample. This can be attributed to the thicker Nb_3Sn layer in the Sn–10Cu–40Zn–2Ti sample. The B_{Kramer} estimated

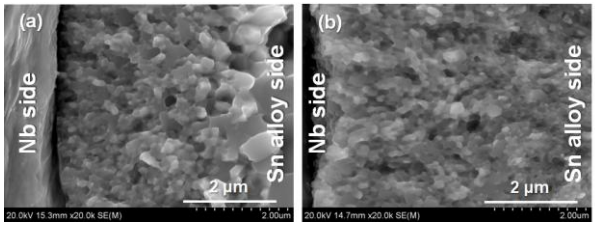

Fig. 6. Grain morphologies of the FG Nb_3Sn area in configurations (a) 1 and (b) 2 using Sn–20Cu–30Zn–2Ti. The average grain sizes are 144 and 114 nm, respectively.

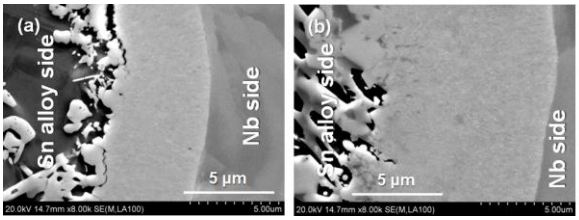

Fig. 7. Grain morphologies of the FG Nb_3Sn area for (a) Sn–20Cu–30Zn–2Ti and (b) Sn–10Cu–40Zn–2Ti in configuration 2.

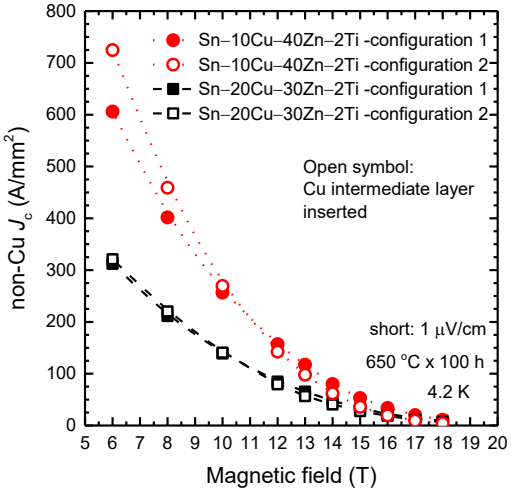

Fig. 8. Non-Cu J_c properties of multifilamentary wires fabricated with Sn–20Cu–30Zn–2Ti and Sn–10Cu–40Zn–2Ti, respectively. Closed symbols and open symbols indicate configuration 1 and 2, respectively.

by extrapolation of $J_c^{0.5}B^{0.25}$ were 20.6 and 21.1 T for Sn–20Cu–30Zn–2Ti wire with and without Cu intermediate layer, and 19.1 and 20.2 T for Sn–10Cu–40Zn–2Ti wire with and without Cu intermediate layer, respectively.

As shown in Fig. 8, J_c–B curves of the wires with and without Cu intermediate layer are crossed. That is presumably attributed to the difference of Ti diffusion to Nb_3Sn phase. As shown in Fig. 5, in the wires with Cu layer, a compound phase of NbSnTiCuZn is formed at the interface of Nb_3Sn and Sn–Cu core. Reportedly, this compound phase tends to trap Ti[26], which would decrease the Ti content in the Nb_3Sn, thereby slightly reducing the B_{c2}. Meanwhile, it is reported that increase in Ti addition to Nb_3Sn tends to slightly coarsen the grain morphology[29],[30], when Ti is doped into Cu-Sn in the precursor, which would decrease the low field J_c properties. Consequently, the J_c curves with and without Cu layer are thought to be crossed.

V. Conclusion

In this study, we presented the effect of hardness and microstructure evolution on Sn alloy fabricated through the co-addition of Cu, Zn, and Ti. This resulted in the precipitation of small compound phases, which increased the hardness of Sn by a factor of three, thereby maintaining drawability. When the composition ratio of Cu to Zn (Cu:Zn) is 20:30 or 10:40, Cu combines with Zn to form stable β-CuZn or γ-CuZn. Zn did not dissolve in the Sn. This would be the reason why dendritic structures do not grow in the Sn alloys.

Controlling the Sn/(Sn + Cu + Zn) ratio at the sub-element level by adding an extra Cu layer between the Sn alloy and the Nb tube is crucial to suppress the CG Nb_3Sn area. The consequent increase in Cu content results in a higher FG-to-CG ratio and a finer grain size. An increase in the Zn content tends to promote Nb_3Sn layer formation.

REFERENCES

[1] A. Ballarino and L. Bottura, "Targets for R&D on Nb_3Sn conductor for high energy physics," *IEEE Transactions on Applied Superconductivity*, vol. 25, no. 3, p. 6000906, Jun. 2015, doi: 10.1109/TASC.2015.2390149.

[2] D. Schoerling *et al.*, "The 16 T Dipole Development Program for FCC and HE-LHC," *IEEE Transactions on Applied Superconductivity*, vol. 29, no. 5, Aug. 2019, doi: 10.1109/TASC.2019.2900556.

[3] A. Ballarino *et al.*, "The CERN FCC conductor development program: a worldwide effort for the future generation of high-field magnets," *IEEE Transactions on Applied Superconductivity*, vol. 29, no. 5, p. 6000709, Aug. 2019, doi: 10.1109/TASC.2019.2896469.

[4] H. Utoh, "Magnet design for JA DEMO," in *Japan-US Workshop on Fusion Reactor Design and Critical Issues of Fusion Engineering*, May 2022. [Online]. Available: https://vltfusion.org/wp-content/uploads/2022/04/Magnet-design-for-JA-DEMO_20220328_HU_v3.pdf

[5] H. Utoh *et al.*, "Design study of superconducting TF coil concept with rectangular conductor layer winding with high manufacturability and insulation reliability for JA DEMO," *presented at MT-27*, p. WED-OR3-201-03, 2021, [Online]. Available: https://indico.cern.ch/event/975584/contributions/4428241/

[6] K. Tobita *et al.*, "Japan's efforts to develop the concept of JA DEMO during the past decade," *Fusion Science and Technology*, vol. 75, no. 5, pp. 372–383, Jul. 2019, doi: 10.1080/15361055.2019.1600931.

[7] J. A. Parrell, Y. Zhang, M. B. Field, P. Cisek, and S. Hong, "High field Nb_3Sn conductor development at Oxford superconducting technology," *IEEE Transactions on Applied Superconductivity*, vol. 13, no. 2 III, pp. 3470–3473, Jun. 2003, doi: 10.1109/TASC.2003.812360.

[8] J. A. Parrell *et al.*, "Internal tin Nb_3Sn conductors engineered for fusion and particle accelerator applications," in *IEEE Transactions on Applied Superconductivity*, Jun. 2009, pp. 2573–2579. doi: 10.1109/TASC.2009.2018074.

[9] M. B. Field, Y. Zhang, H. Miao, M. Gerace, and J. A. Parrell, "Optimizing Nb_3Sn conductors for high field applications," *IEEE Transactions on Applied Superconductivity*, vol. 24, no. 3, p. 6001105, Jun. 2014, doi: 10.1109/TASC.2013.2285314.

[10] S. Kawashima *et al.*, "Development of a high current density distributed tin method Nb_3Sn wire," *IEEE Transactions on Applied Superconductivity*, vol. 30, no. 1, p. 6000105, Jan. 2020, doi: 10.1109/TASC.2019.2915307.

[11] N. Banno, T. Morita, T. Yagai, S. Kawashima, and Y. Murakami, "Fundamental study on the effect of Zn addition into Cu matrix in DT method Nb_3Sn conductors," *IEEE Transactions on Applied Superconductivity*, vol. 30, no. 4, p. 6000705, Jun. 2020, doi: 10.1109/TASC.2020.2972209.

[12] V. R. Nazareth, M. D. Sumption, X. Peng, E. Gregory, M. J. Tomsic, and E. W. Collings, "Characterization of the A15 layer growth and micro structure for varying heat treatments in Nb_3Sn tube type composites," *IEEE Transactions on Applied Superconductivity*, vol. 18, no. 2, pp. 1005–1009, Jun. 2008, doi: 10.1109/TASC.2008.922464.

[13] X. Peng *et al.*, "Strain and magnetization properties of high subelement count tube-type Nb_3Sn strands," *IEEE Transactions on Applied Superconductivity*, vol. 21, no. 3 PART 3, pp. 2559–2562, Jun. 2011, doi: 10.1109/TASC.2010.2100013.

[14] X. Xu, E. Collings, M. Sumption, C. Kovacs, and X. Peng, "The effects of Ti addition and high Cu/Sn ratio on Tube Type $(Nb, Ta)_3Sn$ strands, and a new type of strand designed to reduce unreacted Nb ratio," *IEEE Transactions on Applied Superconductivity*, vol. 24, no. 3, pp. 12–15, 2014, doi: 10.1109/TASC.2013.2291159.

[15] X. Xu, M. D. Sumption, and X. Peng, "Internally oxidized Nb_3Sn strands with fine grain size and high critical current density," *Advanced Materials*, vol. 27, no. 8, pp. 1346–1350, Feb. 2015, doi: 10.1002/adma.201404335.

[16] X. Xu, J. Rochester, X. Peng, M. Sumption, and M. Tomsic, "Ternary Nb_3Sn superconductors with artificial pinning centers and high upper critical fields," *Supercond Sci Technol*, vol. 32, no. 2, p. 02LT01, Jan. 2019, doi: 10.1088/1361-6668/aaf7ca.

[17] X. Xu *et al.*, "APC Nb_3Sn superconductors based on internal oxidation of Nb-Ta-Hf alloys," *Supercond Sci Technol*, vol. 36, no. 3, p. 035012, Mar. 2023, doi: 10.1088/1361-6668/acb17a.

[18] G. Bovone *et al.*, "Effects of the oxygen source configuration on the superconducting properties of internally-oxidized internal-Sn Nb_3Sn wires," *Supercond Sci Technol*, vol. 36, no. 9, p. 095018, Sep. 2023, doi: 10.1088/1361-6668/aced25.

[19] X. Xu, X. Peng, J. Rochester, J. Y. Lee, and M. Sumption, "High critical current density in internally-oxidized Nb_3Sn superconductors and its origin," *Scr Mater*, vol. 186, pp. 317–320, 2020, doi: 10.1016/j.scriptamat.2020.05.043.

[20] I. Pong, S. C. Hopkins, X. Fu, B. A. Glowacki, J. A. Elliott, and A. Baldini, "Microstructure development in Nb_3Sn(Ti) internal tin superconducting wire," *J Mater Sci*, vol. 43, no. 10, pp. 3522–3530, Mar. 2008, doi: 10.1007/s10853-008-2522-4.

[21] N. Banno, T. Morita, Z. Yu, T. Yagai, and K. Tachikawa, "Effect of Zn addition and Ti doping position on the diffusion reaction of internal tin Nb_3Sn conductors," *Supercond Sci Technol*, vol. 32, no. 11, p. 115017, Nov. 2019, doi: 10.1088/1361-6668/ab4632.

[22] X. Xu, M. D. Sumption, and E. W. Collings, "A model for phase evolution and volume expansion in tube type Nb_3Sn conductors," *Supercond Sci Technol*, vol. 26, no. 12, p. 125006, Dec. 2013, doi: 10.1088/0953-2048/26/12/125006.

[23] X. Xu, "Prospects for improving the critical current density of superconducting Nb_3Sn strands via optimization of Nb_3Sn fraction, stoichiometry, and grain size," Ph.D. dissertation, Ohio State University, 2016. [Online]. Available: https://mse.osu.edu/sites/default/files/2022-01/csmm.xingchen_xu_dissertation-1.pdf

[24] C. Segal, C. Tarantini, P. J. Lee, and D. C. Larbalestier, "Improvement of small to large grain A15 ratio in Nb_3Sn PIT wires by inverted multistage heat treatments," *IOP Conf Ser Mater Sci Eng*, vol. 279, no. 1, p. 012019, Dec. 2017, doi: 10.1088/1757-899X/279/1/012019.

[25] N. Banno, "Low-temperature superconductors: Nb_3Sn, Nb_3Al, and NbTi," *Superconductivity*, vol. 6, p. 100047, Jun. 2023, doi: 10.1016/j.supcon.2023.100047.

[26] T. Morita, T. Yagai, and N. Banno, "Impact of Ti-doping position on Nb_3Sn layer formation in internal Sn-processed Nb_3Sn superconducting wires," *Cryogenics (Guildf)*, vol. 122, p. 103420, Mar. 2022, doi: 10.1016/j.cryogenics.2022.103420.

[27] N. Banno, Y. Miyamoto, and K. Tachikawa, "Multifilamentary Nb_3Sn wires fabricated through internal diffusion process using brass matrix," *IEEE Transactions on Applied Superconductivity*, vol. 26, no. 3, p. 6001504, Apr. 2016, doi: 10.1109/TASC.2016.2531123.

[28] C. Sanabria, M. Field, P. J. Lee, H. Miao, J. Parrell, and D. C. Larbalestier, "Controlling Cu-Sn mixing so as to enable higher critical current densities in RRP® Nb_3Sn wires," *Supercond Sci Technol*, vol. 31, no. 6, p. 64001, Apr. 2018, doi: 10.1088/1361-6668/aab8dd.

[29] T. Asano, Y. Iijima, K. Itoh, and K. Tachikawa, "Effects of titanium addition to the niobium core on the composite-processed Nb_3Sn," *Transactions of the Japan Institute of Metals*, vol. 27, no. 3, pp. 204–214, 1986, doi: 10.2320/matertrans1960.27.204.

[30] S. Santra *et al.*, "Insight into the effect of Ti-addition on diffusion-controlled growth and texture of Nb_3Sn intermetallic superconductor phase," *Materialia (Oxf)*, vol. 6, no. January, p. 100276, 2019, doi: 10.1016/j.mtla.2019.100276.